

Wing inertia and whole-body acceleration: an analysis of instantaneous aerodynamic force production in cockatiels (*Nymphicus hollandicus*) flying across a range of speeds

Tyson L. Hedrick, James R. Usherwood and Andrew A. Biewener

Concord Field Station, Museum of Comparative Zoology, Harvard University, 100 Old Causeway Road, Bedford, MA 01730, USA

*Author for correspondence (e-mail: thedrick@oeb.harvard.edu)

Accepted 12 February 2004

Summary

We used a combination of high-speed 3-D kinematics and three-axis accelerometer recordings obtained from cockatiels flying in a low-turbulence wind tunnel to characterize the instantaneous accelerations and, by extension, the net aerodynamic forces produced throughout the wingbeat cycle across a broad range of flight speeds (1–13 m s⁻¹). Our goals were to investigate the variation in instantaneous aerodynamic force production during the wingbeat cycle of birds flying across a range of steady speeds, testing two predictions regarding aerodynamic force generation in upstroke and the commonly held assumption that all of the kinetic energy imparted to the wings of a bird in flapping flight is recovered as useful aerodynamic work. We found that cockatiels produce only a limited amount of lift during upstroke (14% of downstroke lift) at slower flight speeds (1–3 m s⁻¹). Upstroke lift at intermediate flight speeds (7–11 m s⁻¹) was moderate, averaging 39% of downstroke lift. Instantaneous aerodynamic forces were greatest near mid-downstroke. At the end of each half-stroke, during

wing turnaround, aerodynamic forces were minimal, but inertial forces created by wing motion were large. However, we found that the inertial power requirements of downstroke (minimum of 0.29±0.10 W at 7 m s⁻¹ and maximum of 0.56±0.13 W at 1 m s⁻¹) were consistent with the assumption that nearly all wing kinetic energy in downstroke was applied to the production of aerodynamic forces and therefore should not be added separately to the overall power cost of flight. The inertial power requirements of upstroke (minimum of 0.16±0.04 W at 7 m s⁻¹ and maximum of 0.35±0.11 W at 1 m s⁻¹) cannot be recovered in a similar manner, but their magnitude was such that the power requirements for the upstroke musculature (minimum of 54±13 W kg⁻¹ at 7 m s⁻¹ and maximum of 122±35 W at 1 m s⁻¹) fall within the established range for cockatiel flight muscle (<185 W kg⁻¹).

Key words: cockatiel, *Nymphicus hollandicus*, flight, inertia, accelerometer.

Introduction

Our main goals in this study were twofold: (1) to investigate the variation in instantaneous aerodynamic force production during the wingbeat cycle of birds flying across a range of steady speeds and (2) to quantify the inertial costs of flapping flight, along with an estimate of the amount of wing kinetic energy (E_k) that is transferred to whole body E_k or potential energy (E_p). In doing so, we sought to test the current assumption in the avian flight literature that all of the E_k imparted to the wings is recovered as useful aerodynamic work (e.g. Pennycuick and Lock, 1976; Pennycuick et al., 2000; Askew et al., 2001; Tobalske et al., 2003). If this is the case, the energy required to accelerate the wing does not represent an incremental cost to the overall energy requirement for flight of a bird because the E_k added to the wing eventually acts to support or propel the bird. However, while this assumption is longstanding, experimental support is generally limited to slow flight (Pennycuick and Lock, 1976; Van den Berg and Rayner,

1995; Askew et al., 2001; Usherwood et al., 2003) and, in a largely theoretical study of hovering hummingbirds, is contradictory (Weis-Fogh, 1972). Nevertheless, in accordance with others (Pennycuick et al., 2000; Askew et al., 2001; Tobalske et al., 2003), we hypothesize that the cockatiel's wing E_k during downstroke is fully recovered to increase the bird's E_k or E_p and does not add to its energy requirements for flight.

Whereas force production during locomotion in terrestrial animals is confined to stride phases during which the feet are in contact with the ground, forces in aquatic or aerial locomotion may be produced whenever the fluid and animal move in relation to one another. Additionally, the instantaneous magnitude and direction of the forces produced in terrestrial locomotion may be readily quantified with a force plate or similar device. No equivalent technology exists for fluid locomotion, although different experimental and modeling approaches provide some of the same information.

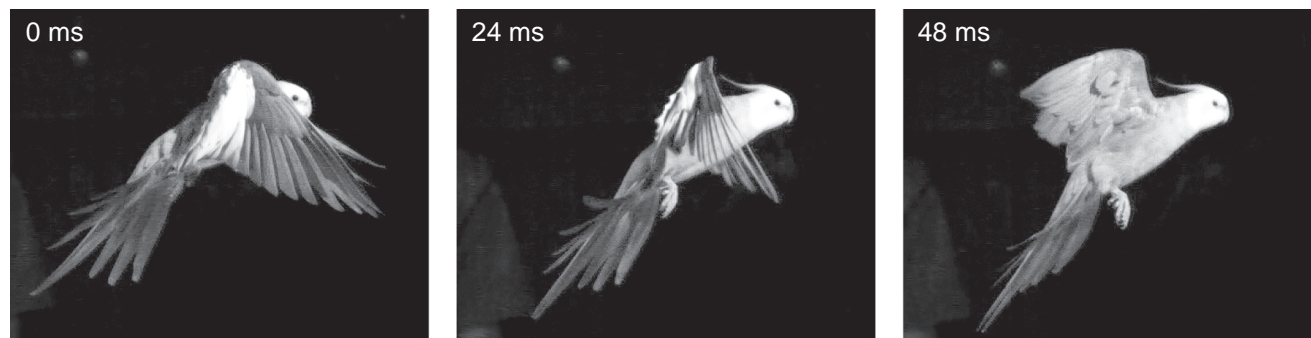


Fig. 1. These images, taken from a high-speed recording of a cockatiel flying at 1 m s^{-1} , show the tip-reversal upstroke. In the first frame, the wing has already reversed direction and the humerus has been elevated. In the second frame, the primary feathers have rotated slightly to create gaps between successive feathers. Between the second and third frames, the rotated primaries sweep upward as the wrist joint extends. By the third frame, the primaries have been rotated back into their standard orientation and the wing has begun to move forward as well as upward.

Fluid visualization *via* digital particle image velocimetry (DPIV) allows measurement of some of these forces, but the results are typically interpreted over full- or half-cycle intervals due to the difficulty of visualizing flows close to the animal (Stamhuis and Videler, 1995; Drucker and Lauder, 1999; Spedding et al., 2003). Physical modeling allows detailed investigation of the time-course and magnitude of the locomotor forces but has thus far been most effectively applied to the relatively simple flight surfaces, kinematics and low Reynolds number regime of insect flight (Ellington et al., 1996; Dickinson et al., 1999). Computational fluid dynamics (CFD) models offer the possibility of quantifying fluid flow and force production over the entire surface of the animal but have thus far been limited to cases where existing physical models can be used to validate the CFD results (Liu et al., 1998; Ramamurti and Sandberg, 2002; Sun and Tang, 2002).

In the present study, we employed a third approach. We used accelerometers attached to the dorsal body center of cockatiels (*Nymphicus hollandicus* Kerr), together with high-speed 3-D kinematics, to measure the net instantaneous forces produced during complete wingbeat cycles. We obtained these measurements as the birds flew in a low-turbulence wind tunnel (Hedrick et al., 2002) across a range of steady flight speeds. Our approach followed that of Bilo et al. (1984), who examined several wingbeats of a pigeon (*Columba livia*) in steady fast flight. The accelerometers measured the net effect of internal (inertial) and external (aerodynamic) forces acting on the bird's body. Inertial forces are generated by oscillation of the bird's wings about its body, whereas aerodynamic forces result from the interactions between the bird and the surrounding fluid. To obtain estimates of net aerodynamic forces, we therefore used 3-D kinematics of wing motion to quantify and remove the inertial forces experienced by the bird's body.

Measuring the resultant aerodynamic forces produced within a wingbeat cycle allowed us to test two predictions of wing stroke function during upstroke. First, at slow flight speeds of approximately $0\text{--}3 \text{ m s}^{-1}$, the cockatiels employ a 'tip-reversal' type of upstroke in which the wing flexed at the wrist early in

the upstroke, the proximal portion of the wing was elevated, and the distal portion of the wing then swept around and upward with the feathers rotated on their axes (Fig. 1). This type of upstroke has been hypothesized to allow the individual feathers to act as airfoils, producing lift as they sweep back (Brown, 1963; Aldridge, 1986; Norberg, 1990; Azuma, 1992). However, because our previous kinematic analysis of flight in cockatiels (Hedrick et al., 2002) did not reveal any obvious upward movement of the body during upstroke, we hypothesized that a tip-reversal upstroke would not produce substantial lift or thrust in this species.

In addition to the tip-reversal upstroke, various investigators (Spedding, 1987; Rayner, 1993; Hedrick et al., 2002; Spedding et al., 2003) have suggested that the wing may be aerodynamically active during upstroke at medium to fast flight speeds ($5\text{--}11 \text{ m s}^{-1}$ in cockatiels). By positioning the wing at a positive angle of attack during upstroke and allowing their own forward velocity to drive flow past the airfoil, birds may be able to generate lift with consequent additional drag during the upstroke. Because our previous work on cockatiels (Hedrick et al., 2002) provided some support for this, we hypothesized that cockatiels would employ a lift-producing upstroke at faster flight speeds ($5\text{--}11 \text{ m s}^{-1}$). Recent flow visualization (DPIV) analysis of the wake of a thrush nightingale (*Luscinia luscinia* L.; Spedding et al., 2003) has also shown that the amount of energy added to the wake during upstroke gradually increased with flight speed in that species. This suggests that upstroke lift may also gradually increase with speed. However, our previous kinematic analysis (Hedrick et al., 2002) indicates that upstroke lift in cockatiels may decline again at the fastest speed (13 m s^{-1}) achieved during experiments in the Harvard-CFS wind tunnel.

Materials and methods

Animals and flight training

Four cockatiels (*Nymphicus hollandicus* Kerr; body mass $87.3 \pm 7.4 \text{ g}$; mean \pm S.D.; Table 1) were purchased from a local licensed animal vendor and housed in a $1.7 \text{ m} \times 2.7 \text{ m} \times 3.3 \text{ m}$

Table 1. Morphometric data for the cockatiels (*Nymphicus hollandicus*) and experimental conditions

Variable	Mean \pm S.D.
Body mass (g)	87.28 \pm 7.36
Estimated pectoralis mass (g)	9.10 \pm 0.77
Estimated supracoracoideus mass (g)	1.41 \pm 0.12
Estimated deltoideus major mass (g)	0.43 \pm 0.04
Wingspan (cm)	45.5 \pm 2.0
Wing chord (cm)	5.7 \pm 0.5
Air temperature ($^{\circ}$ C)	22.44 \pm 3.07
Air pressure (kPa)	102.6 \pm 0.8
Air density (kg m^{-3})	1.21 \pm 0.03

$N=4$ in all cases. Muscle mass estimates were calculated from linear regressions of muscle mass vs body mass for cockatiels used in prior experiments at the Concord Field Station. Muscle masses are for individual muscles.

indoor aviary at the Concord Field Station animal care facility (Bedford, MA, USA), where they were provided with food and water *ad libitum*. The birds were trained to fly over a range of speeds from 1 m s^{-1} to 15 m s^{-1} in the Concord Field Station wind tunnel (Hedrick et al., 2002). Training lasted one month, comprising a minimum of five 20-min bouts of flight training per week. All individuals tended to fly in the upper forward quadrant of the working section of the wind tunnel. Cockatiels learned to fly at a steady speed in the wind tunnel in 2–4 days and were then exercised for at least three additional weeks to expand the speed range over which they would fly steadily prior to data recording. The trained cockatiels were willing to fly for at least 10 min without rest at 9 m s^{-1} . At very fast ($\geq 13 \text{ m s}^{-1}$) and slow ($\leq 3 \text{ m s}^{-1}$) speeds, the duration of flights that the birds were willing to sustain was typically ≤ 1 min. The maximum steady speed of each bird was defined as the highest speed at which it would voluntarily maintain its position in the wind tunnel for 30 s. All training and experimental procedures were approved by the Harvard University Institutional Animal Care and Use Committee.

Flight kinematics

Flight trials were recorded using three synchronized, high-speed digital video cameras [one Photron Fastcam-X 1280 PCI (Photron USA Inc., San Diego, CA, USA) and two Redlake PCI 500 (Redlake Inc., San Diego, CA, USA) operating at $250 \text{ frames s}^{-1}$ with a shutter speed of 1/1000th of a second. The Photron camera was placed above and behind the wind tunnel flight chamber; the two Redlake cameras were positioned on the side of the tunnel opposite the operator with one lateral to the bird and the other postero-lateral (Fig. 2A). The camera data were synchronized with the accelerometer signals by recording the cameras' digital stop trigger together with the accelerometer outputs *via* an A/D converter (Axoscope Digidata 1200; Axon Instruments Inc., CA, USA). The cameras were calibrated using the modified direct linear

transformation (DLT) technique with a 70 point calibration frame (measuring $0.457 \text{ m} \times 0.967 \text{ m} \times 0.900 \text{ m}$ in xyz coordinate space) that was recorded at the end of each set of trials (Hatze, 1988). Trials were recorded at flight speeds of $1\text{--}13 \text{ m s}^{-1}$ in 2 m s^{-1} intervals. Flight speed sequence was not restricted to a particular order, and the birds were allowed to rest between trials as necessary to maintain satisfactory performance (typically 2–5 min of sustained flight).

Three points (dorsal and ventral surfaces of the shoulder, wrist and tip of the ninth primary) were marked on the right wing of each bird using 5 mm-diameter dabs of white correction fluid. The dried correction fluid was marked with a small black central dot. In addition, three points defining two orthogonal axes were attached to the accelerometers using two short lengths (2.5 cm) of wire, with a known orientation to the accelerometer sensitive axes (Fig. 2B). These axes were used to orient the accelerometers in the global reference frame later in analysis (see below).

Flight sequences consisting of a minimum of four successive wingbeats with minimal lateral and vertical movement within the flight chamber (velocity relative to the flight chamber of $<0.5 \text{ m s}^{-1}$) were selected from the video data and the points noted above digitized using custom software written in MATLAB v. 6.5 (The Mathworks Inc., Natick, MA, USA). In the few cases (3 of 28) where sufficient sequential wingbeats with minimal change in wind tunnel position were not available, we selected additional wingbeats from the recorded flight sequence, digitizing at least four wingbeats for each individual at each speed.

The raw coordinate data obtained from the digitized trials were resolved into a single 3-D space using the DLT coefficients derived from the calibration frame (Hatze, 1988). In addition to resolving the dorsal and lateral 2-D camera views into a single 3-D space, the modified DLT method also corrects for parallax and other linear and lens distortions. Individual points having a DLT root mean square error (RMSE) two standard deviations greater than the median RMSE for that point (approximately 4% of the points) were considered outliers and removed prior to analysis. Median RMSE ranged from 1.19 mm for the orthogonal axis markers to 1.49 mm for the ninth primary tip. Occasionally, a point was not in the view of at least two of the three cameras (approximately 7% of all points digitized), resulting in a gap in the reconstructed point sequence. After the digitized coordinate data were filtered, missing or dropped points were interpolated with a quintic spline fit to known RMSE using the 'Generalized Cross Validatory/Spline' (GCVSPL) program (Woltring, 1986). This method uses the RMSE from the DLT reconstruction to filter the positional data and then fills any gaps with a quintic spline interpolation. The results from this technique were similar to those obtained by smoothing the positional data using a 37 Hz digital Butterworth low-pass filter. However, the quintic spline method also allows direct calculation of velocity and acceleration derivatives from the spline curves, providing the most accurate method for obtaining higher order derivatives from positional data (Walker, 1998).

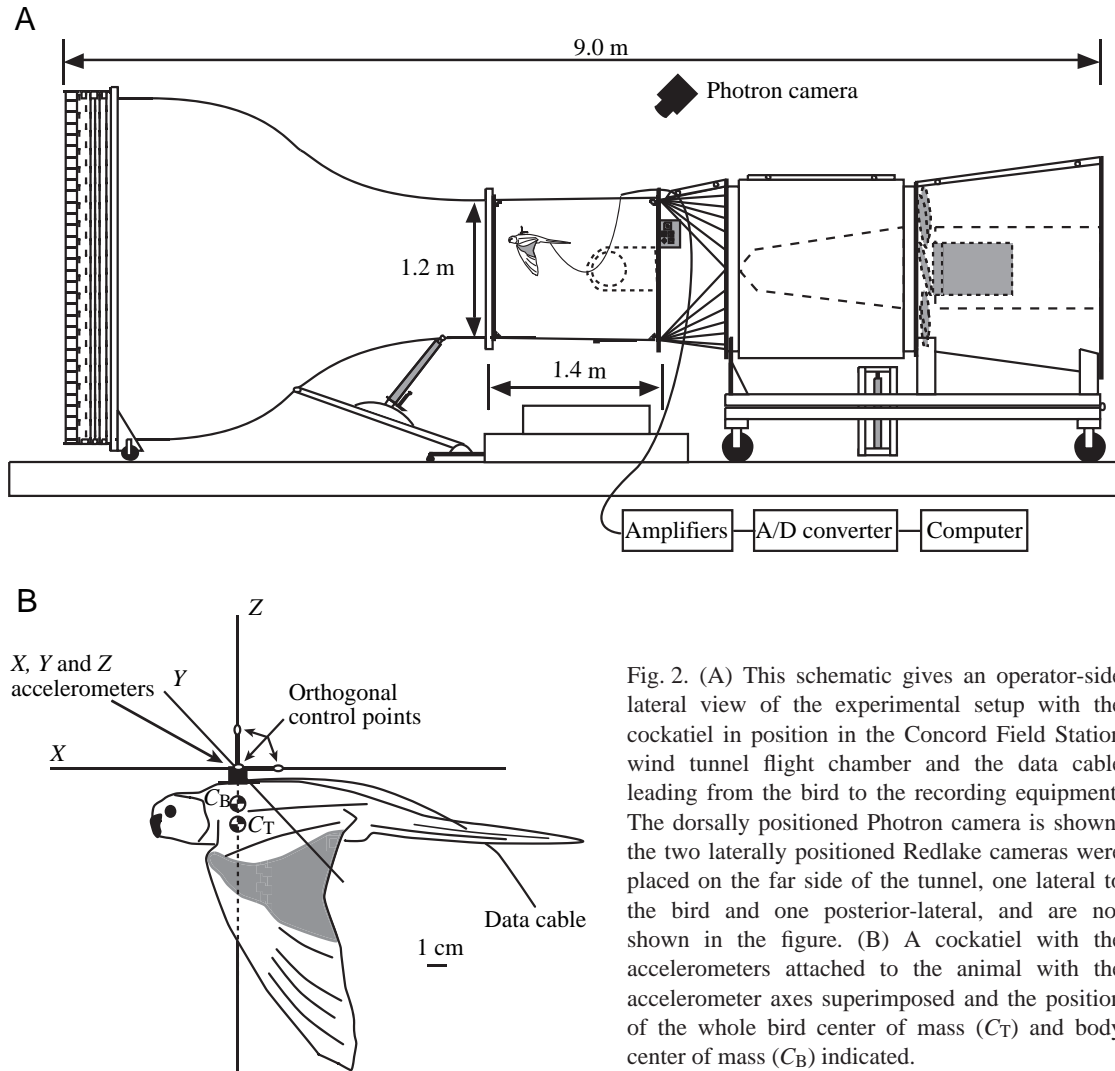


Fig. 2. (A) This schematic gives an operator-side lateral view of the experimental setup with the cockatiel in position in the Concord Field Station wind tunnel flight chamber and the data cable leading from the bird to the recording equipment. The dorsally positioned Photron camera is shown; the two laterally positioned Redlake cameras were placed on the far side of the tunnel, one lateral to the bird and one posterior-lateral, and are not shown in the figure. (B) A cockatiel with the accelerometers attached to the animal with the accelerometer axes superimposed and the position of the whole bird center of mass (C_T) and body center of mass (C_B) indicated.

Accelerometers

We measured instantaneous accelerations of the cockatiels *via* a block of three accelerometers (1 EGA2-10 dual axis accelerometer and 1 EGA-10 single axis accelerometer; Entran Devices Inc., Fairfield, NJ, USA) mounted at orthogonal axes and attached to the dorsal midline of the cockatiels just above the estimated center of mass. The center of mass position was estimated by first locating it in a frozen, wingless cockatiel cadaver by hanging the specimen at various angles, then relating this to the position on the experimental animal estimated *via* visual and tactile landmarks. The accelerometers were anchored to the dorsal midline by suturing the accelerometer base plate to the intervertebral ligaments with two loops of 3-0 silk suture while the bird was under light anesthesia (isoflurane; Fig. 2B). Accelerometer signals were collected through a lightweight (5.6 g) multi-lead cable that ran a distance of 1 m from the accelerometers on the animal to a small (0.75 cm diameter) opening at the top of the wind tunnel's working section. This lightweight cable connected to a heavier, shielded cable outside the flight chamber that ran to

the recording amplifiers (Micromasurements 2120 bridge amplifiers; Vishay Intertechnology Inc., Malvern, PA, USA). The amplifier outputs were sampled by the A/D converter at 5 kHz and stored on a computer for subsequent analysis.

The mass of the accelerometers and the portion of the data cable supported by the bird was 11.4 g, approximately 13% of the total body mass of the bird. Measurements of the drag produced by the cable and attached accelerometer ranged from 0.05 N at 1 m s^{-1} to 0.23 N at 13 m s^{-1} . These measurements were made without an associated cockatiel; drag from the accelerometer and cable may therefore differ somewhat when associated with a bird's body. However, the effect of this drag, when related to the inertial and aerodynamic forces produced over the entire downstroke and upstroke phases, can be expected to be small and of negligible significance to how the patterns of inertial and aerodynamic force relate to each other. The cockatiels typically ignored the accelerometers and data cable while flying in the wind tunnel. The presence of the accelerometers did result in a reduction in the maximum flight speed we were able to record in the wind tunnel (from 15 m s^{-1}

to 13 m s⁻¹), probably due to the additional drag from the cable and accelerometers. Flight duration and the position within the tunnel that each bird selected, however, were unaffected.

After each recording session, we recorded accelerometer calibration voltages by positioning each accelerometer's sensitive axis at 0°, 45°, 90° and 180° with respect to gravity. An accelerometer calibration equation was calculated from least squares regression of the recorded voltages and the expected accelerations of g , 0.707 g , 0 and $-g$. In all cases, the r^2 for the calibration regression was ≥ 0.99 . After calibration, we used the position information obtained by digitizing the three markers attached to the accelerometer block to rotate the accelerometer outputs from their native 'bird-fixed' orientation on the dorsal surface of the animal to the standard global coordinate space defined by the camera calibration frame. Rotations were performed *via* a series of Euler angle transformations:

$$[\ddot{X}_B \quad \ddot{Y}_B \quad \ddot{Z}_B] = [\ddot{A}_1 \quad \ddot{A}_2 \quad \ddot{A}_3] \begin{bmatrix} \cos(\alpha) & -\sin(\alpha) & 0 \\ \sin(\alpha) & \cos(\alpha) & 0 \\ 0 & 0 & 1 \end{bmatrix} \\ \begin{bmatrix} \cos(\beta) & 0 & \sin(\beta) \\ 0 & 1 & 0 \\ -\sin(\beta) & 0 & \cos(\beta) \end{bmatrix} \begin{bmatrix} 1 & 0 & 0 \\ 0 & \cos(\gamma) & -\sin(\gamma) \\ 0 & \sin(\gamma) & \cos(\gamma) \end{bmatrix}, \quad (1)$$

where $[\ddot{X}_B \quad \ddot{Y}_B \quad \ddot{Z}_B]$ are the total center of body accelerations in the global coordinate space and $[\ddot{A}_1 \quad \ddot{A}_2 \quad \ddot{A}_3]$ are the three orthogonal accelerations recorded by the accelerometers. Angle α is the angle about the Z (vertical) axis between \ddot{A}_1 and the X (forward) axis in the global coordinate space, β is the angle about the Y (lateral) axis between \ddot{A}_3 and the global Z axis (following the initial transformation with α) and γ is the angle about the X (forward) axis between \ddot{A}_2 and the global Y axis (following the transformations with α and β).

Although the inertial forces produced by wing motion cannot accelerate the bird's center of mass (C_T), they can produce accelerations at the center of the body (C_B ; Fig. 2B), above which the accelerometers were attached and that will be included in the accelerometer recordings. Following Bilo et al. (1984), we accounted for these accelerations of C_B due to inertial forces (subsequently referred to as inertial accelerations) by reconstructing them from the 3-D wing kinematics (see below) and subtracting them from the accelerometer recordings.

Reconstruction of the inertial accelerations requires a mass distribution for the wing as well as the wing's kinematics. We created a standard cockatiel wing mass distribution by sectioning and weighing wings from three cockatiels. The resulting standard cockatiel wing was composed of 18 slices, each of which was 1.3 cm wide, and included both the actual section mass and an estimated virtual mass predicted from the volume of air accelerated with the wing (Fig. 3). The virtual mass contributed 12.6% to the total wing mass (Fig. 3B) and 25.8% to the moment of inertia (Fig. 3A) for a fully extended wing. The total moment of inertia for the outstretched

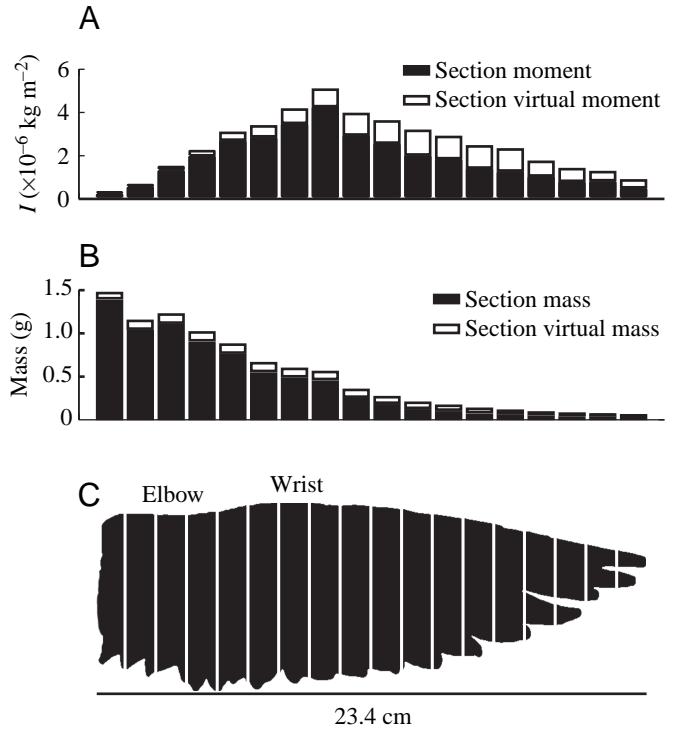


Fig. 3. (A) This histogram shows the contribution of each wing section to the overall mass moment of inertia (I) of the wing. The moment of inertia calculation employs the sum of the actual and virtual masses shown in B. Each wing section was 1.3 cm wide. (B) This histogram shows the mass and estimated virtual mass of the individual wing sections. Total mass of the standard wing was 8.32 g; the s.d. between the masses of the three original wings was 0.66 g. (C) A silhouette of the standard cockatiel wing divided into 18 sections. The sections incorporating the elbow and wrist joints are labeled.

standardized wing shown here was $4.02 \times 10^{-5} \text{ kg m}^{-2}$; the standard deviation between the three individual wings was $3.12 \times 10^{-6} \text{ kg m}^{-2}$. Virtual mass for each section was computed using the following equation from Norberg (1990):

$$m_{i,v} = \frac{1}{4} \pi \rho w_i c_i, \quad (2)$$

where $m_{i,v}$ is the virtual (or added) mass of section i , ρ is air density, w_i is the width of section i , and c_i is its chord.

Our model treats each wing section as a point mass. This is a reasonable assumption given the concentration of mass in each strip at the leading edge in the bone and muscle rather than in the feathers extending posterior and the large number of wing slices we employed (Van den Berg and Rayner, 1995). We merged the mass information from the standard wing with the 3-D kinematics by computing the position of each wing strip in each video frame, then distributing the appropriate number of strips between the shoulder, wrist and wingtip. We then derived the acceleration of each wing section in the global frame of reference by taking the 2nd derivative of a quintic spline fit between the successive positions of each wing strip. The resulting X-, Y- and Z-axis section accelerations were used

to reconstruct the inertial accelerations with equations 3–7 (below). Lastly, we subtracted the predicted inertial accelerations from the accelerometer recordings leaving only the accelerations due to aerodynamic forces. We assumed that the two wings operate symmetrically and that the Y -axis inertial accelerations cancel each other.

The predicted inertial accelerations of C_B were calculated from equations 10–15a of Bilo et al. (1984), restated here for convenience as equations 3–7:

$$\ddot{Z}_{B,I} = \frac{-2\sum m_i \ddot{z}_i}{m_T}, \quad (3)$$

where $\ddot{Z}_{B,I}$ is the vertical (Z -axis) acceleration of C_B due to inertial forces, m_i is the mass of the i th wing section, \ddot{z}_i is the vertical acceleration of the i th section in a frame of reference fixed to the bird, m_T is the bird's total body mass (including the mass of the accelerometers and supported cable) and '2' accounts for the two wings. This equation may be reached by first considering the acceleration of C_T in terms of the acceleration of C_B and the wing segments:

$$\ddot{Z}_T = \frac{m_B \ddot{Z}_B + 2\sum m_i \ddot{z}_i}{m_T}, \quad (4)$$

where \ddot{Z}_T is the vertical acceleration of C_T , \ddot{Z}_B is the acceleration of C_B (the quantity measured by the accelerometers) and \ddot{z}_i is the vertical acceleration of the i th wing section. The acceleration C_T can be translated into a local frame of reference with Z_B , the vertical position of C_B , at zero *via*:

$$\ddot{Z}_T = \ddot{Z}_T - \ddot{Z}_B = \frac{m_B \ddot{Z}_B + 2\sum m_i \ddot{z}_i}{m_T}, \quad (5)$$

where \hat{Z}_T is the vertical position of C_T in the local frame of reference and \hat{Z}_B is the vertical position of C_B (which is fixed at zero in the local frame of reference). We also define two additional relationships between the accelerations of C_T and C_B :

$$\ddot{Z}_T = \ddot{Z}_{B,E} \quad (6)$$

and

$$\ddot{Z}_B = \ddot{Z}_{B,E} + \ddot{Z}_{B,I}, \quad (7)$$

where $\ddot{Z}_{B,E}$ is the vertical acceleration of C_B due to external forces and $\ddot{Z}_{B,I}$ is the vertical acceleration of C_B due to inertial forces. Equations 6 and 7 may be substituted into equation 5 to give equation 3. This analysis assumes that the inertial forces act through C_B and therefore produce no torque. A similar progression can be followed to calculate $\ddot{X}_{B,I}$, the horizontal inertial acceleration of C_B . Note that the aerodynamic forces calculated from $\ddot{Z}_{B,E}$ and other external accelerations encompass all aerodynamic forces acting on the bird, including drag from the data cable and accelerometer.

Inertial power

We calculated the inertial power requirements for downstroke and upstroke by taking the change in wing E_k from

the start of each half-stroke to its point of maximum E_k and dividing these energies by the duration of the entire wingbeat cycle. Wing E_k was computed from the mass distribution and kinetic analysis described above. We consider only the work of wing acceleration in both upstroke and downstroke because deceleration is unlikely to require substantial metabolic input in any circumstance due to the high metabolic efficiency of vertebrate muscle when actively generating force to absorb energy (Abbott et al., 1952). By contrast, we calculate power from the entire wingbeat duration because the muscle contractions involved in powering the movements of the wing occur over an entire wingbeat cycle.

Wing kinetic energy recovery

Current models of forward flight in birds assume that the inertial power requirements for downstroke do not incur any metabolic cost because the wing E_k is recovered as aerodynamic work done to support or propel the bird (Pennycuik, 1996; Askew et al., 2001; Tobalske et al., 2003). This is presumed to occur in the latter half of downstroke as the wing loses kinetic energy while doing aerodynamic work to produce forces (lift and thrust) that support and propel the bird. Following Askew et al. (2001), we assume that if the aerodynamic work required to produce the observed whole-body accelerations exceeds the wing E_k then all energy is transferred. Only in cases where the wing E_k exceeds aerodynamic work does the inertial power incur a metabolic cost. This analysis ignores any additional muscle work done during the wing deceleration phase but provides a simple benchmark to evaluate the importance of inertial power requirements in downstroke.

To carry out this analysis, it was necessary to estimate the aerodynamic work required to produce the observed aerodynamic forces. We employed the aerodynamic model described in equations 2–7 of Hedrick et al. (2003) to estimate the instantaneous aerodynamic power output based on the bird's wing kinematics and whole-body accelerations. For the purposes of comparison with wing E_k , we computed the aerodynamic work performed during the period of wing deceleration in downstroke. This can be summarized as:

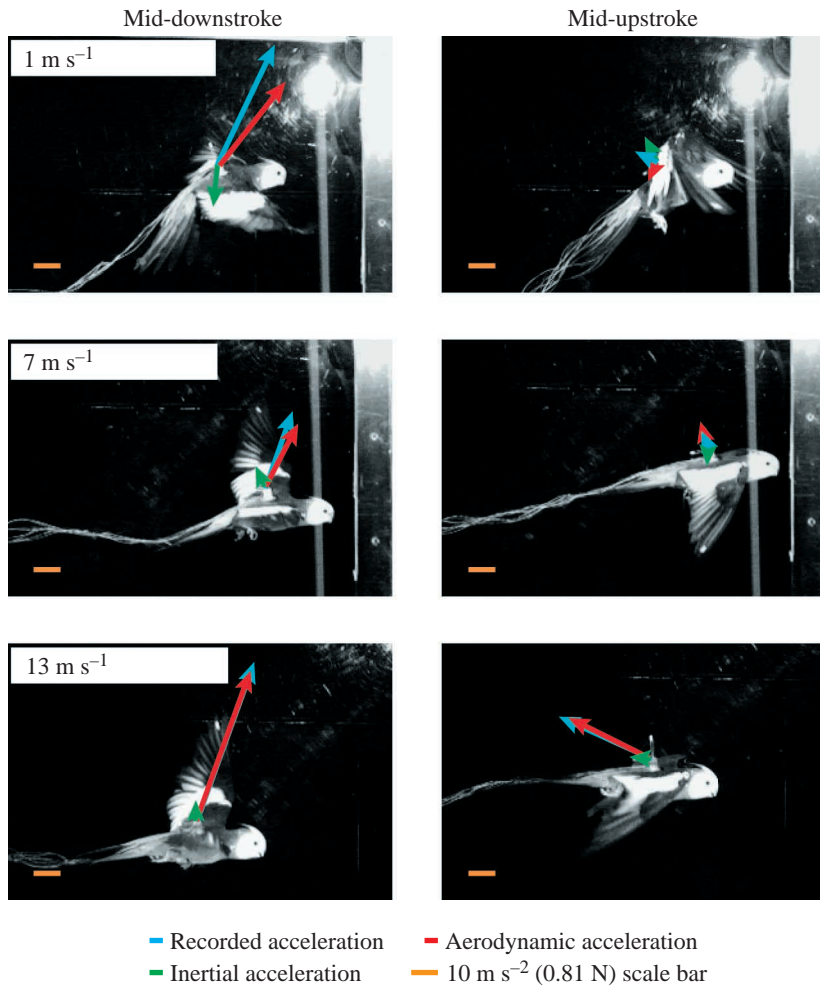
$$E_{k,rd} = \Delta E_{k,w} - E_{aero}, \quad (8)$$

where $E_{k,rd}$ is the kinetic energy during downstroke that exceeds the aerodynamic work performed, $\Delta E_{k,w}$ is the change in wing E_k from its maximum to its value at the end of downstroke, and E_{aero} is the aerodynamic work performed over the same time interval. The transfer of wing E_k to aerodynamic work during upstroke wing deceleration has not been proposed and is not considered here. Instead, we assume that upstroke is powered entirely by the supracoracoideus and deltoideus major muscles.

Results

Within-wingbeat variation in aerodynamic and inertial forces

The magnitude of vertical and horizontal whole-body acceleration resulting from aerodynamic forces varied



continuously throughout the wingbeat cycle and across speeds. Forces during downstroke were similar among birds, speeds and wingbeats, with maximum aerodynamic forces typically falling near mid-downstroke while forces during upstroke were of lower magnitude but varied more widely. Fig. 4 shows a snapshot of the vertical and horizontal net force vectors at the mid-downstroke and mid-upstroke postures at three different flight speeds. Note the decrease in the overall magnitude of downstroke aerodynamic force at the intermediate speed (7 m s⁻¹). These snapshots are expanded in Fig. 5 (lower panels) to show the mean acceleration patterns produced by all four cockatiels across the range of flight speeds tested. While inertial forces were small in comparison to aerodynamic forces at the mid-downstroke and mid-upstroke phases shown in Fig. 4, they were greatest during wing turnaround at the end of upstroke and downstroke, as can be seen in Fig. 5. Peak inertial forces were larger at slow and fast flight speeds when compared with intermediate speeds and became closer in magnitude to the aerodynamic forces as speed increased. Nevertheless, peak inertial forces were always less than peak aerodynamic forces, being less than 50% of peak aerodynamic forces at 1 m s⁻¹ and 3 m s⁻¹ and between 50% and 60% at all other flight speeds.

Fig. 4. Here, we superimpose some of the typical instantaneous acceleration vectors from mid-downstroke and mid-upstroke on the lateral-view high-speed video footage. The same cockatiel is used in all frames and the vector scale is the same in each case. Note that the inertial acceleration vectors are small in size here because the wing is typically at maximum velocity when near mid-stroke; inertial accelerations were much more pronounced at other points in time such as the ends of upstroke and downstroke. In upstroke at faster flight speeds, lift and drag forces tended to vary together and were either both small, as shown in the 7 m s⁻¹ upstroke, or both larger, as shown in the 13 m s⁻¹ upstroke. The scale bar indicates an acceleration of 10 m s⁻², equivalent to a force of 0.81 N applied to the cockatiel's whole body mass. Note that the aerodynamic acceleration vectors include drag from the data cable and accelerometers.

Despite continuous variation in acceleration throughout a wingbeat, certain features of the acceleration profile of the wingbeat cycle remained consistent across flight speeds. We found that maximum horizontal acceleration occurred at a cycle phase of 0.65 (zero being defined as the start of upstroke, and 1.0 the end of downstroke) and maximum vertical acceleration occurred at a phase of 0.74. Both of these occurred near the kinematic mid-downstroke (phase of 0.73), with the wings fully outstretched and horizontal to the bird. These phases did not vary significantly with flight speed ($F=0.38$ and $F=1.78$ for vertical and horizontal acceleration phase, respectively; $P>0.05$, repeated-measures ANOVA) but were significantly different from one another ($P<0.05$, t -test of individual means).

We also observed that the initial two-thirds of downstroke generally produced positive (forward) thrust, while the latter third resulted in negative (rearward) thrust. The negative thrust was associated with a large angle of incidence adopted by the wing late in downstroke as the wing supinated prior to upstroke. Positive (upward) lift was produced over the entire downstroke at all speeds. By contrast, lift and thrust production during upstroke generally varied more, especially at slow and fast flight speeds. During the upstroke, lift and drag tended to vary together. For example, at 7 m s⁻¹ (Fig. 5B), the cockatiels reduced both lift and drag whereas at 13 m s⁻¹ (Fig. 5C) lift production was coupled with increased drag. Finally, net accelerations due to aerodynamic forces were near zero at the end of downstroke at all speeds, despite the rapid wing rotations that occurred at this time during slower flight speeds (1–3 m s⁻¹; Fig. 5).

Mean aerodynamic forces in upstroke and downstroke

As expected, the mean magnitude of whole-body

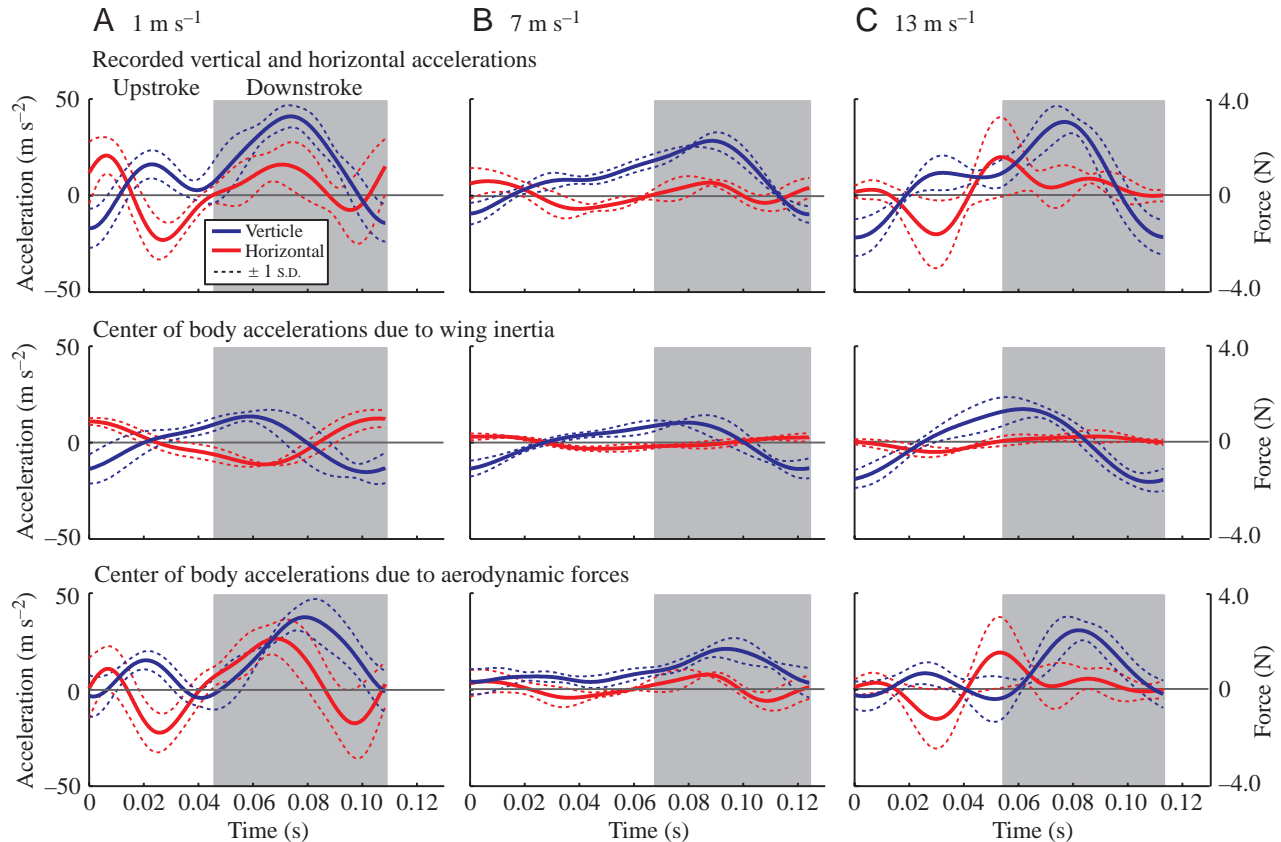


Fig. 5. A set of inter-individual mean curves showing the patterns of acceleration and wing movement across a single wingbeat from the start of upstroke to the end of downstroke across a range of speeds. Light gray regions denote downstroke. Solid lines indicate the inter-individual mean response, while broken lines show the mean ± 1 s.d. A, B and C correspond to results from flight speeds of 1 m s^{-1} , 7 m s^{-1} and 13 m s^{-1} , respectively. None of the birds in this study was able to sustain faster flight speeds with the recording equipment attached. Note that the aerodynamic acceleration vectors include drag from the data cable and accelerometers. Removing drag would not change the mean horizontal acceleration over a wingbeat cycle but would probably reduce the instantaneous magnitude of the acceleration. The maximum drag measured on the accelerometer and cable (at 13 m s^{-1}) would generate an acceleration of approximately 2.6 m s^{-2} , much less than the observed acceleration magnitudes.

acceleration resulting from aerodynamic forces in both the vertical and horizontal directions varied significantly between upstroke and downstroke ($P < 0.001$ for both vertical and horizontal, paired t -test). The mean vertical acceleration during upstroke and downstroke also varied significantly with speed ($P < 0.05$, $F = 3.81$ and $F = 4.52$ for downstroke and upstroke, respectively; repeated-measures ANOVA). Differences in mean vertical acceleration between upstroke and downstroke were minimized at intermediate flight speeds and maximized at both faster and slower speeds (Fig. 6). The same trends also characterize the mean horizontal accelerations. Furthermore, the specialized tip-reversal upstroke employed by cockatiels at slow flight speeds (1 m s^{-1} and 3 m s^{-1}) was not associated with large net accelerations in any direction.

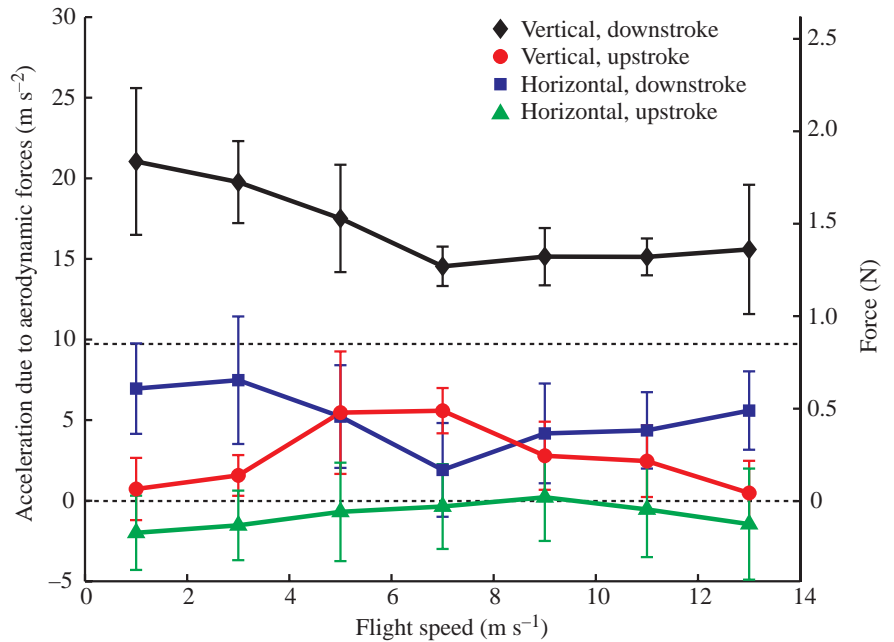
Wing kinetic energy and the inertial power requirements of flight

The inertial work required to accelerate the wing varied significantly with flight speed downstroke ($P < 0.01$, $F = 4.18$; repeated-measures ANOVA) but not upstroke ($P > 0.05$;

Fig. 7A). However, because of speed-related variation in the duration of upstroke relative to downstroke, wing inertial power varied significantly with speed for both upstroke and downstroke ($P < 0.05$, $F = 3.81$ and $P < 0.01$, $F = 6.49$, respectively; repeated-measures ANOVA; Fig. 7B). Not surprisingly, wing inertial work and power during the downstroke exceeded that during the upstroke. This results from the wings' outstretched configuration and increased moment of inertia during the downstroke compared with their flexed configuration during upstroke. However, we did find that in slow-speed flight ($1\text{--}3 \text{ m s}^{-1}$) the exceptionally brief duration of wing acceleration in upstroke elevated the mean power output to a level nearly equal to that in downstroke.

These inertial work requirements translate into substantial mass-specific inertial power requirements when measured over a complete wingbeat cycle. Downstroke pectoralis mass-specific inertial power requirements averaged 24.0 W kg^{-1} across the entire speed range (Fig. 8). This represents 21.9% of the cockatiels' pectoralis power output, based on the results of Tobalske et al. (2003). Nevertheless, the maximum wing E_k

Fig. 6. Mean vertical and horizontal accelerations during downstroke and upstroke resulting from aerodynamic forces plotted *versus* flight speed. The values shown are means \pm 1 s.d. for the four birds. Vertical and horizontal upstroke and downstroke accelerations differed significantly between stroke phases ($P < 0.001$, paired t -test), and vertical accelerations differed significantly across speeds. Note that maintaining position in the wind tunnel requires that aerodynamic forces produce a mean vertical acceleration of $+9.81 \text{ m s}^{-2}$ (to counter gravity) and a horizontal acceleration of 0 m s^{-2} ; there was a slight tendency toward forward acceleration in the cockatiels, especially at faster flight speeds.



developed during downstroke *in excess* of the aerodynamic work performed during wing deceleration ($E_{k,rd}$) was negative at speeds less than 7 m s^{-1} and only slightly positive at faster speeds, averaging 7.25 W kg^{-1} or 7.0% of pectoralis power output for speeds of $>7 \text{ m s}^{-1}$.

Muscle mass-specific inertial power requirements for upstroke were greater than those for downstroke due to the large mass difference between the upstroke and downstroke musculature (Table 1). Assuming that the wings' acceleration and E_k during upstroke are achieved *via* contraction of the supracoracoideus and deltoideus major muscles, upstroke mass-specific inertial power reached a maximum of 122 W kg^{-1} at a flight speed of 1 m s^{-1} (Fig. 8) and averaged 89 W kg^{-1} over all flight speeds. At slower flight speeds

($1\text{--}5 \text{ m s}^{-1}$), upstroke mass-specific inertial power was similar to the pectoralis mass-specific power output required for aerodynamic force production (Fig. 8). At faster speeds, upstroke inertial power declined somewhat relative to pectoralis power output.

Discussion

While analysis of the instantaneous locomotor forces produced by flying animals will likely remain difficult, our application of high-speed digital video and 3-D kinematic reconstruction to the accelerometry techniques developed by Bilo et al. (1984) provide an additional method through which these forces can be measured. Although this study covered a much wider range of speeds and wingbeats than the earlier study and employed cockatiels rather than pigeons, both studies examined instantaneous force production throughout a wingbeat cycle, and some general comparisons between the two are possible. Bilo et al. (1984) measured forces on a 395 g pigeon flying at 11 m s^{-1} , with accelerations reported as forces applied to the center of mass. The larger mass and

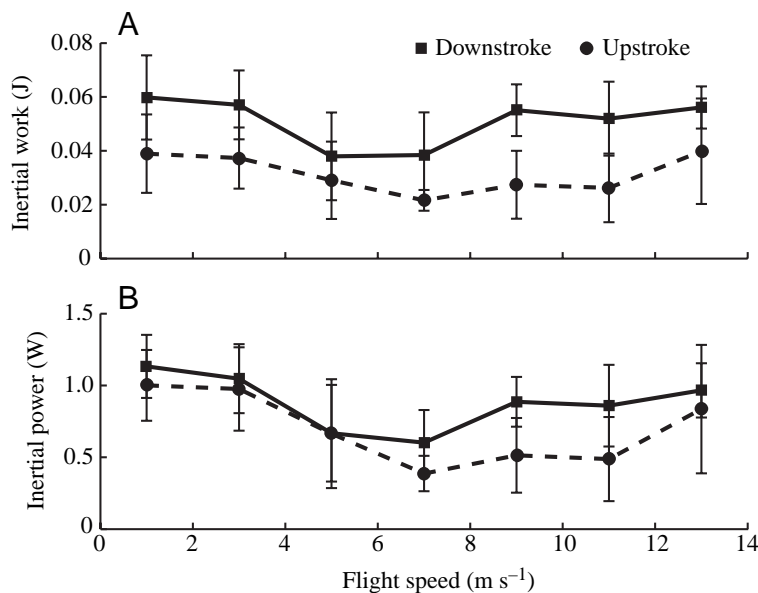
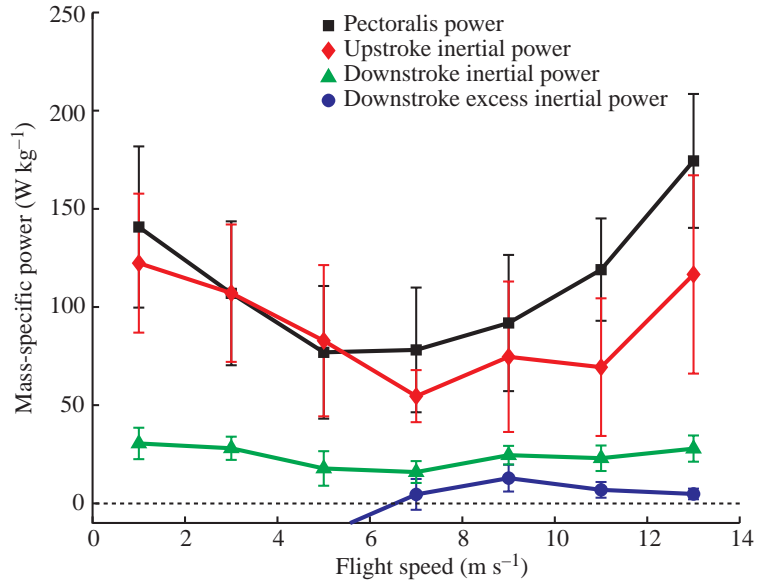


Fig. 7. Mean inertial work (A) and inertial power (B) associated with wing acceleration during upstroke and downstroke plotted *versus* flight speed. Note that while inertial work in upstroke is less than in downstroke at all speeds, this is not the case for inertial power. The reduced duration of upstroke at slower flight speeds increases the upstroke inertial power to the point where it is nearly equal to the downstroke power. As we found previously in cockatiels (Hedrick et al., 2003), changes in wingbeat duration were entirely due to changes in upstroke duration, as downstroke duration did not vary.

Fig. 8. A comparison of the measured cockatiel pectoralis mass-specific muscle power output (black) reported by Tobalske et al. (2003) with three measures of the mass-specific inertial power requirements of flapping flight. The upstroke mass-specific inertial power (red) is the peak wing kinetic energy developed in upstroke divided by the mass of the upstroke musculature and the wingbeat duration. This is the best measure of the muscle power required for upstroke. The downstroke mass-specific inertial power (green) is the peak wing kinetic energy developed in downstroke divided by the pectoralis mass and wingbeat duration. The downstroke excess inertial power is the peak wing kinetic energy in downstroke with the aerodynamic work done during wing deceleration subtracted, i.e. $E_{k,rd}$. This sum was converted to a mass-specific power by dividing by the pectoralis mass and wingbeat duration. The muscle masses used to calculate mass-specific powers are given in Table 1.



greater wing loading of the pigeon probably resulted in faster maximum and typical flight speeds than the cockatiels employed in the present study; the pigeon's larger size certainly resulted in greater aerodynamic forces. However, presuming that Bilo et al. (1984) used the flight speed at which the pigeon was most comfortable in the wind tunnel, the results should be compared with cockatiels flying at 7 m s^{-1} , the speed at which the cockatiels flew most readily. Additionally, we converted the forces from Bilo et al. (1984) back to accelerations for comparison with the cockatiels since the mean acceleration over a wingbeat cycle will be the same for all birds in steady, level flight.

Given these assumptions, we can compare the following results from the two studies: (1) the magnitude of inertial accelerations, (2) the magnitude of the aerodynamic accelerations and (3) the timing of peak accelerations during the wingbeat cycle. The pigeon was reported to produce inertial accelerations that were approximately 25–33% of the magnitude of the aerodynamic accelerations. In cockatiels, the inertial accelerations were nearly equivalent to their aerodynamic equivalents in the vertical direction and were approximately 50% in the horizontal direction at a flight speed of 7 m s^{-1} . This discrepancy is probably explained by three factors: (1) the inclusion of added mass in the determination of cockatiel wing moment of inertia, (2) differences in camera recording frequency and (3) the scaling of wing size with body size. The added mass component elevates the cockatiel moment of inertia and peak inertial acceleration by 26%. Removing this component would decrease the cockatiel horizontal acceleration into the same range as that of the pigeon, for which added mass was not included (Bilo et al., 1984), but would not fully account for the differences in vertical inertial acceleration. Higher imaging frequencies will more accurately estimate the peak accelerations and therefore result in greater inertial forces. We recorded at 250 Hz whereas

Bilo et al. (1984) recorded at 80 Hz. This difference probably explains at least part of the remaining discrepancy in inertial accelerations. Any remaining differences are likely to be the result of differences in wing morphology and moment of inertia between the two species. Cockatiels have relatively long wings with a high moment of inertia for their body mass ($4.02 \times 10^{-5} \text{ kg m}^{-2}$ in the present study). This is well above that of other bird species of a similar body mass (Van den Berg and Rayner, 1995), although less than the value of $1.65 \times 10^{-4} \text{ kg m}^{-2}$ for the much larger pigeon studied by Bilo et al. (1984).

While we expect the pigeon to produce larger absolute aerodynamic forces due to its greater mass, whole-body accelerations of the cockatiels and pigeon should be comparable in magnitude. However, the peak horizontal and vertical accelerations of the pigeon reached nearly 40 m s^{-2} compared with 22.6 m s^{-2} peak vertical and 7.4 m s^{-2} peak horizontal accelerations in the cockatiels. Because vertical and horizontal accelerations over the entire wingbeat cycle must average near 9.81 m s^{-2} and 0 m s^{-2} , respectively, for both species, the lower peak values for the cockatiels indicate a smoother wingbeat cycle with less variation in acceleration at this flight speed. We believe this may reflect the cockatiels' use of an aerodynamically active upstroke, which we discuss below. At faster and slower speeds, peak accelerations in the cockatiels approached 40 m s^{-2} , comparable with those in the pigeon.

The timing of peak accelerations was similar between the two studies. Bilo et al. (1984) reported that peak aerodynamic accelerations occurred near mid-downstroke as the wings passed through the horizontal plane, with peak vertical accelerations slightly preceding peak horizontal accelerations. In the cockatiels, we also found peak accelerations near mid-downstroke, although peak horizontal accelerations slightly preceded peak vertical accelerations.

Lift production during upstroke

By obtaining 3-D kinematic and whole-body acceleration data, we confirmed our hypothesis that the tip-reversal upstroke employed by cockatiels in slow flight ($1\text{--}3\text{ m s}^{-1}$) is not an important source of lift or thrust, contrary to some previous hypotheses (Brown, 1963; Aldridge, 1986; Norberg, 1990; Azuma, 1992). The tip-reversal upstroke did result in a slight upward acceleration, but this came at the cost of a larger rearward acceleration (Figs 5, 6). The magnitude of both these accelerations was much less than those produced during the downstroke. Although the tip-reversal does not make an important contribution to weight support, it was surprisingly effective at minimizing the inertial work required to accelerate the wing in upstroke (Fig. 7A). Despite the reduced duration and increased amplitude of upstroke at slow flight speeds, the wings' peak kinetic energy was not significantly greater than that at other speeds ($P > 0.05$; repeated-measures ANOVA). In a tip-reversal upstroke, the proximal portion of the wing is accelerated in early upstroke while the distal portion is allowed to travel freely. Later in upstroke, the proximal wing is decelerated while the distal wing is accelerated. By accelerating different portions of the wing at different times in upstroke the tip-reversal motion effectively reduces the wing's peak kinetic energy and the work required to accelerate the wing. This probably permits a more rapid upstroke than would otherwise be possible, given the limited size of the cockatiel upstroke musculature. Thus, the tip-reversal upstroke appears to be an effective means for long-winged birds to rapidly elevate their wings without a substantial increase in inertial work and negative (downward or rearward) aerodynamic forces that might otherwise be produced by upward wing motion.

We also confirmed our hypothesis that upstroke lift at intermediate flight speeds provides more substantial weight support than at slower and very high speeds. At flight speeds from 5 m s^{-1} to 11 m s^{-1} , aerodynamic forces in upstroke produced upward accelerations that exceeded 2 m s^{-2} but were still less than the 9.81 m s^{-2} required to counter gravity (Fig. 6). Upstroke lift production was greatest at 5 m s^{-1} and 7 m s^{-1} , resulting in vertical accelerations as high as 6 m s^{-2} . At these speeds, mean vertical acceleration during downstroke was correspondingly reduced. As a result, upstroke lift was 35% of that produced in downstroke. These results confirm expectations based on our earlier work (Hedrick et al., 2002) and are also consistent with the gradual increase in upstroke wake energy with flight speed recently found in the thrush nightingale (Spedding et al., 2003).

The energy source used to power aerodynamic force production during upstroke is most likely the bird's own kinetic and potential energy. This is because the upstroke musculature is of small size and is not well positioned to produce upward or forward aerodynamic forces. To estimate the changes in whole-body energy during upstroke, we integrated the instantaneous accelerations using initial velocities taken from the kinematics. This analysis showed generally similar decrements in whole-body kinetic and

potential energies, consistent with their role in providing upstroke aerodynamic force. However, when examined more closely, we found that the cockatiels favored a slightly greater kinetic energy loss at flight speeds below 9 m s^{-1} and greater potential energy loss at flight speeds above 9 m s^{-1} .

Downstroke inertial power

Our results for the inertial power requirements of downstroke generally support the currently accepted view that the energy required to accelerate the wing in downstroke is wholly subsumed within the aerodynamic power requirements of avian flight (Pennycuick et al., 2000; Askew et al., 2001; Hedrick et al., 2003). Although our calculations show that there is kinetic energy in excess of aerodynamic work at speeds of $>7\text{ m s}^{-1}$, this excess kinetic energy is negligible in comparison to the overall power requirements for flight at these higher speeds (Fig. 8). Our simple test of the importance of wing kinetic energy (equation 8) assumes that the pectoralis muscle does no work during the latter half of downstroke as the wing decelerates. However, prior *in vivo* measurements of pectoralis force and length change obtained from cockatiels and other species show that this is not the case – the avian pectoralis continues to shorten and produce force throughout the downstroke (Dial et al., 1997; Biewener et al., 1998; Hedrick et al., 2003).

Re-examination of our previous results for cockatiel pectoralis power output (Hedrick et al., 2003) shows that $24.2 \pm 4.6\%$ (mean \pm S.D.) of the work done by the pectoralis is performed as the wing decelerates during the latter half of the downstroke. Also, this fraction does not vary systematically with flight speed. Thus, equation 8 should contain an additional term adding the work done by the pectoralis muscle to the aerodynamic work and wing kinetic energy. At slow flight speeds ($1\text{--}5\text{ m s}^{-1}$), the work done by the pectoralis during wing deceleration does not affect the conclusion that inertial power requirements are unimportant because the aerodynamic work greatly exceeded wing kinetic energy (Fig. 8). However, at flight speeds greater than 5 m s^{-1} , the wing kinetic energy and aerodynamic work done during wing deceleration were similar in magnitude. Consequently, accounting for work performed by the pectoralis during downstroke wing deceleration increases the likelihood that not all of the wing kinetic energy can be usefully transferred to the surrounding air and that a significant fraction must be absorbed or stored through other mechanisms at moderate to fast flight speeds.

An attractive possibility for elastic energy storage is the long robust tendon of the supracoracoideus muscle. Electromyographic recordings of the supracoracoideus of pigeons (Dial, 1992) show that it is activated during the terminal phase of the downstroke. This suggests that, in addition to developing force to decelerate and elevate the wing, its tendon may also store and recover excess kinetic energy of the wing. Future study of the cockatiel supracoracoideus will be needed to examine this possibility. Otherwise, although reduced at faster speeds, any excess inertial kinetic energy

during downstroke should be added to the overall power requirements of flight for this species.

Upstroke inertial power

Although the inertial power required to accelerate the wing in upstroke averaged only 14% of the cockatiels' total aerodynamic power requirements, this inertial power requirement is probably incremental to the bird's aerodynamic power requirements. Unlike the downstroke, no aerodynamic transfer mechanism has been proposed. It is difficult to envision how the upwardly moving wing of a bird can produce lift or thrust without the use of muscles and while losing velocity during the second half of the upstroke, when inertial kinetic energy would need to be recovered. Elastic strain energy stored in the supracoracoideus tendon could be used to power the initial acceleratory phase of the upstroke, reducing the amount of additional energy input *via* the upstroke muscles. Although a reasonable candidate for this, until now energy storage in the supracoracoideus tendon has not been demonstrated and should not therefore be considered to account for the inertial power required for upstroke.

In addition to the upstroke musculature, aerodynamic forces might also be used to elevate the wing at the beginning of upstroke. However, this would not eliminate the inertial power required for upstroke because aerodynamic forces require their own energy source. As we discussed above, this is most likely derived from losses in the bird's own potential or kinetic energy. Even so, this energy ultimately must be produced by the bird's downstroke musculature (pectoralis) during the subsequent wing beat cycle. Furthermore, our comparison of the wings' kinetic energy in upstroke relative to concurrent losses in whole-body kinetic and potential energy suggests that all whole-body energy losses are applied to weight support rather than wing elevation.

Elastic energy storage offers another possible mechanism for minimizing the additional energy required for upstroke. As in downstroke, it is possible that the kinetic energy is stored elastically as the wing decelerates, most likely in the tendinous attachment of the pectoralis to the humerus and within the pectoralis muscle itself. However, recordings of muscle force and length change in the pectoralis of cockatiels (Tobalske et al., 2003) indicate that the muscle produces little force as the wing decelerates. Consequently, although some storage may occur late in upstroke it does not appear to be large enough to account for the loss in wing kinetic energy.

Aerodynamic force production and wing rotation

Our recordings of whole-body acceleration also allow us to assess indirectly whether cockatiels obtain useful lift from wing rotation when flying at slow speeds. Unsteady aerodynamic force production *via* wing rotation has been described in insect flight (Dickinson et al., 1999) and, for flies, accounts for a substantial fraction of the lift needed for weight support. Given the rapid supination and pronation of the wing that occurs in cockatiels, and other birds, during the end of the downstroke and upstroke at slower flight speeds, it seems

possible that birds may also obtain some benefit from wing rotation. However, we found that net aerodynamic forces typically approached zero during stroke reversal at the lower flight speeds (1–3 m s⁻¹; Fig. 5), when wing rotation is most pronounced. This suggests that aerodynamic mechanisms associated with wing translation, rather than wing rotation, predominate in the generation of flight power of cockatiels, as well as other birds.

Future work

The use of accelerometer techniques first developed by Bilo et al. (1984) and employed here to analyze the inertial and aerodynamic power requirements of the steady flapping flight of cockatiels over a range of speeds provides considerable insight into the mechanisms for aerodynamic power production and kinetic energy exchange. Such an approach might also be used to analyze patterns of aerodynamic force production during unsteady, maneuvering flight to better understand the aerodynamic mechanisms by which birds maneuver, particularly at slow speeds. In combination with recordings of muscle activation, force production and length change, measurements of whole-body acceleration may allow a more detailed investigation of how birds produce and control the forces required for maneuvering flight. As we have seen in our analysis of cockatiels during steady flight across a range of speeds, interactions between wing inertia, elastic energy recovery and muscle work, and the aerodynamic power requirements of flight remain uncertain. Experiments that artificially vary wing inertia while recording pectoralis length change and force production may also provide better insight into the importance of wing inertia in flight and how the behavior of a power-producing muscle–tendon system operates under an inertial load. Inertial loads have recently been shown to accentuate the peak power output of the plantaris muscle and tendon in jumping bullfrogs (Roberts and Marsh, 2003). A similar mechanism could operate in the pectoralis muscle of birds during flapping flight if the pectoralis tendon/aponeurosis can store and release adequate elastic strain energy and this energy can be effectively transferred to the air while producing useful aerodynamic force. Finally, the resolution and recording frequency limitations of current high-speed video technologies make derivation of whole-body accelerations from video unreliable in most circumstances, encouraging the use of accelerometers. However, video technologies are improving rapidly and may soon allow sufficiently accurate acceleration measurements without requiring the use of accelerometers.

Summary

The combination of high-speed 3-D kinematics and three-axis accelerometer data allowed us to explore the timing and magnitude of net aerodynamic force production throughout the wingbeat cycle of cockatiels flying across a range of steady speeds. Our results reveal that the proposed mechanisms for aerodynamic force production during upstroke in slow flight result in little net force. However, useful aerodynamic force production during upstroke at intermediate speeds was

observed, consistent with our earlier estimates of circulation and lift production (Hedrick et al., 2002) and with the latest flow visualization analysis of steady avian flight (Spedding et al., 2003). At speeds from 7 m s^{-1} to 11 m s^{-1} , net aerodynamic forces during upstroke acted in an upward and rearward direction, as expected. Detailed examination of the inertial power requirements for flapping flight in cockatiels generally supported the commonly held assumption that the inertial kinetic energy of the wing during the downstroke is converted into useful aerodynamic work and need not represent an incremental cost to the power required for flight. This was best supported at slower flight speeds, where inertial power requirements were greatest but aerodynamic power requirements were also large. At faster flight speeds, excess downstroke kinetic energy was observed. We believe that this excess kinetic energy may be recovered by elastic storage within the tendon of the supracoracoideus muscle, but this remains to be confirmed. Our analysis of the kinetic energy imparted to the wing during upstroke indicates that the majority is probably dissipated and should be added to the total power requirement for flapping avian flight. However, some fraction of this energy may also be stored and recovered within elastic structures of the pectoralis.

List of symbols

\ddot{A}_1	acceleration measured by accelerometer axis 1
\ddot{A}_2	acceleration measured by accelerometer axis 2
\ddot{A}_3	acceleration measured by accelerometer axis 3
C_B	center of mass of the bird's wingless body including accelerometers
c_i	chord of wing section i
C_T	center of mass of the whole bird including accelerometers
E_{aero}	work done on the air to support and propel the bird, also referred to as aerodynamic work
E_k	kinetic energy
$E_{k,\text{rd}}$	wing E_k in downstroke in excess of the aerodynamic work done as the wing decelerates
$\Delta E_{k,w}$	change in wing E_k over the specified time interval
E_p	potential energy
I	mass moment of inertia
m_i	mass of wing section i
$m_{i,v}$	added mass of wing section i
m_T	the bird's total body mass, including accelerometers
w_i	width of wing section i
\ddot{X}_B	net horizontal acceleration of C_B
$\ddot{X}_{B,I}$	horizontal acceleration of C_B due to inertial forces
\ddot{Y}_B	net lateral acceleration of C_B
Z_B	vertical position of C_B
\dot{Z}_B	vertical position of C_B in the local frame of reference (fixed at zero)
\ddot{Z}_B	net vertical acceleration of C_B
$\ddot{Z}_{B,E}$	vertical acceleration of C_B due to external forces
$\ddot{Z}_{B,I}$	vertical acceleration of C_B due to inertial forces
\ddot{z}_i	vertical acceleration of the i th wing section

\ddot{z}_i	vertical acceleration of wing section i in the local frame of reference
\ddot{Z}_T	vertical acceleration of C_T
\dot{Z}_T	vertical position of C_T in the local frame of reference
\ddot{Z}_B	vertical acceleration of C_B in the local frame of reference
\dot{Z}_T	vertical acceleration of C_T in the local frame of reference
α	rotation angle about the Z (vertical) axis
β	rotation angle about the Y (lateral) axis
γ	rotation angle about the X (horizontal) axis
ρ	air density

We would like to thank Pedro Ramirez for caring for the cockatiels and Bret Tobalske for valuable discussion on these research topics, as well as the constructive comments of two referees. Also, special thanks to Pierre Tresfort (Tresfort Metal Works) and Quentin Spendrup (SMJ, Inc.) for quality construction of the wind tunnel. This work was supported by NSF IBN-0090265 to A.A.B.

References

- Abbott, B. C., Bigland, B. and Ritchie, J. M. (1952). The physiologic cost of negative work. *J. Physiol. Lond.* **117**, 380-390.
- Aldridge, H. D. J. N. (1986). Kinematics and aerodynamics of the greater horseshoe bat (*Rhinolopus ferrumequinum*) in horizontal flight at various flight speeds. *J. Exp. Biol.* **126**, 479-497.
- Askew, G. N., Marsh, R. L. and Ellington, C. P. (2001). The mechanical power output of the flight muscles of blue-breasted quail (*Coturnix chinensis*) during take-off. *J. Exp. Biol.* **204**, 3601-3619.
- Azuma, A. (1992). *The Biokinetics of Flying and Swimming*. New York: Springer.
- Biewener, A. A., Corning, W. R. and Tobalske, B. W. (1998). In vivo pectoralis muscle force-length behavior during level flight in pigeons (*Columba livia*). *J. Exp. Biol.* **201**, 3293-3307.
- Bilo, D., Lauck, A. and Nachtigall, W. (1984). Measurement of linear body accelerations and calculation of the instantaneous aerodynamic lift and thrust in a pigeon flying in a wind tunnel. In *Biona-Report 3* (ed. W. Nachtigall). Stuttgart, Gustav Fischer.
- Brown, R. H. J. (1963). The flight of birds. *Biol. Rev.* **38**, 460-489.
- Dial, K. P. (1992). Activity patterns of the wing muscles of the pigeon (*Columba livia*) during different modes of flight. *J. Exp. Biol.* **262**, 357-373.
- Dial, K. P., Biewener, A. A., Tobalske, B. W. and Warrick, D. R. (1997). Mechanical power output of bird flight. *Nature* **390**, 67-70.
- Dickinson, M. H., Lehmann, F.-O. and Sane, S. P. (1999). Wing rotation and the aerodynamic basis of insect flight. *Science* **284**, 1881-2044.
- Drucker, E. and Lauder, G. (1999). Locomotor forces on a swimming fish: three-dimensional vortex wake dynamics quantified using digital particle image velocimetry. *J. Exp. Biol.* **202**, 2393-2412.
- Ellington, C. P., Van den Berg, C., Willmott, A. P. and Thomas, A. L. R. (1996). Leading-edge vortices in insect flight. *Nature* **384**, 626-630.
- Hatze, H. (1988). High-precision three-dimensional photogrammetric calibration and object space reconstruction using a modified DLT approach. *J. Biomech.* **21**, 533-538.
- Hedrick, T. L., Tobalske, B. W. and Biewener, A. A. (2002). Estimates of circulation and gait change based on a three-dimensional kinematic analysis of flight in cockatiels (*Nymphicus hollandicus*) and ringed turtle-doves (*Streptopelia risoria*). *J. Exp. Biol.* **205**, 1389-1409.
- Hedrick, T. L., Tobalske, B. W. and Biewener, A. A. (2003). How cockatiels (*Nymphicus hollandicus*) modulate pectoralis power output across flight speeds. *J. Exp. Biol.* **206**, 1363-1378.
- Liu, H., Ellington, C. P., Kawachi, K., Van den Berg, C. and Willmott, A. P. (1998). A computational fluid dynamic study of hawkmoth hovering. *J. Exp. Biol.* **201**, 461-477.
- Norberg, U. M. (1990). *Vertebrate Flight: Mechanics, Physiology, Morphology, Ecology and Evolution*. Berlin: Springer-Verlag.

- Pennycuik, C. J.** (1996). Wingbeat frequency of birds in steady cruising flight: new data and improved predictions. *J. Exp. Biol.* **199**, 1613-1618.
- Pennycuik, C. J., Hedenström, A. and Rosén, M.** (2000). Horizontal flight of a swallow (*Hirundo rustica*) observed in a wind tunnel, with a new method for directly measuring mechanical power. *J. Exp. Biol.* **203**, 1755-1765.
- Pennycuik, C. J. and Lock, A.** (1976). Elastic energy storage in primary feather shafts. *J. Exp. Biol.* **64**, 677-689.
- Ramamurti, R. and Sandberg, W. C.** (2002). A three-dimensional computational study of the aerodynamic mechanisms of insect flight. *J. Exp. Biol.* **205**, 1507-1518.
- Rayner, J. M. V.** (1993). On the aerodynamics and the energetics of vertebrate flapping flight. *Cont. Math.* **141**, 351-400.
- Roberts, T. J. and Marsh, R. L.** (2003). Probing the limits to muscle-powered accelerations: lessons from jumping bullfrogs. *J. Exp. Biol.* **206**, 2567-2580.
- Spedding, G. R.** (1987). The wake of a kestrel (*Falco tinnunculus*) in flapping flight. *J. Exp. Biol.* **127**, 59-78.
- Spedding, G. R., Rosén, M. and Hedenström, A.** (2003). A family of vortex wakes generated by a thrush nightingale in free flight in a wind tunnel over its entire natural range of flight speeds. *J. Exp. Biol.* **206**, 2313-2344.
- Stamhuis, E. and Videler, J.** (1995). Quantitative flow analysis around aquatic animals using laser sheet particle image velocimetry. *J. Exp. Biol.* **198**, 283-294.
- Sun, M. and Tang, J.** (2002). Unsteady aerodynamic force generation by a model fruit fly wing in flapping motion. *J. Exp. Biol.* **205**, 55-70.
- Tobalske, B. W., Hedrick, T. L., Dial, K. P. and Biewener, A. A.** (2003). Comparative power curves in bird flight. *Nature* **421**, 363-366.
- Usherwood, J. R., Hedrick, T. L. and Biewener, A. A.** (2003). The aerodynamics of avian take-off from direct pressure measurements in Canada geese (*Branta canadensis*). *J. Exp. Biol.* **206**, 4051-4056.
- Van den Berg, C. and Rayner, J. M. V.** (1995). The moment of inertia of bird wings and the inertial power requirement for flapping flight. *J. Exp. Biol.* **198**, 1655-1664.
- Walker, J. A.** (1998). Estimating velocities and accelerations of animal locomotion: a simulation experiment comparing numerical differentiation algorithms. *J. Exp. Biol.* **201**, 981-995.
- Weis-Fogh, T.** (1972). Energetics of hovering flight in hummingbirds and in *Drosophila*. *J. Exp. Biol.* **56**, 79-104.
- Wottring, H. J.** (1986). A FORTRAN package for generalized, cross-validatory spline smoothing and differentiation. *Adv. Eng. Software* **8**, 104-113.